Circulation: Heart Failure

ORIGINAL ARTICLE

Overexpression of ATP5F1A in Cardiomyocytes Promotes Cardiac Reverse Remodeling

Mengda Xu, MD, PhD*; Hang Zhang, MD, PhD*; Yuan Chang, MD, PhD*; Xiumeng Hua, MD, PhD; Xiao Chen, MASc; Yixuan Sheng, MASc; Dan Shan, PhD; Mengni Bao, MASc; Shengshou Hu, MD, PhD; Jiangping Song, MD, PhD

BACKGROUND: The mechanism of cardiac reverse remodeling (CRR) mediated by the left ventricular assist device remains unclear. This study aims to identify the specific cell type responsible for CRR and develop the therapeutic target that promotes CRR.

METHODS: The nuclei were extracted from the left ventricular tissue of 4 normal controls, 4 CRR patients, and 4 no cardiac reverse remodeling patients and then subjected to single-nucleus RNA sequencing for identifying key cell types responsible for CRR. Gene overexpression in transverse aortic constriction and dilated cardiomyopathy heart failure mouse model (C57BL/6J background) and pathological staining were performed to validate the results of single-nucleus RNA sequencing.

RESULTS: Ten cell types were identified among 126 156 nuclei. Cardiomyocytes in CRR patients expressed higher levels of *ATP5F1A* than the other 2 groups. The macrophages in CRR patients expressed more anti-inflammatory genes and functioned in angiogenesis. Endothelial cells that elevated in no cardiac reverse remodeling patients were involved in the inflammatory response. Echocardiography showed that overexpressing *ATP5F1A* through cardiomyocyte-specific adeno-associated virus 9 demonstrated an ability to improve heart function and morphology. Pathological staining showed that overexpressing *ATP5F1A* could reduce fibrosis and cardiomyocyte size in the heart failure mouse model.

CONCLUSIONS: The present results of single-nucleus RNA sequencing and heart failure mouse model indicated that *ATP5F1A* could mediate CRR and supported the development of therapeutics for overexpressing *ATP5F1A* in promoting CRR.

Key Words: heart failure ■ heart-assist devices ■ macrophages ■ myocytes, cardiac

The prognosis of heart failure (HF) remains poor despite aggressive medical and surgical treatment.[1] Some patients with HF can restore the structure and function of the heart after being supported with the left ventricular assist device (LVAD), namely, cardiac reverse remodeling (CRR). However, the mechanisms of CRR have not yet been fully elucidated.

During HF, the cell content and function undergo significant changes, and all these changes could affect CRR. Normally, a small number of macrophages are present in the heart. Macrophages can be divided into 2 subtypes: CCR2$^+$ (C-C chemokine receptor type 2) macrophages and CCR2$^-$ macrophages. The level of CCR2$^+$ macrophages is elevated in patients with HF, and immunofluorescence staining shows that no cardiac reverse remodeling (NCRR) patients possessed more CCR2$^+$ macrophages than CRR patients.[2] Changes of cardiomyocytes, the most abundant cells in the heart, also affect CRR. The MPC (mitochondrial pyruvate carrier), which transported pyruvate into the mitochondria, increased after LVAD support in CRR patients, but the level of MPC remained decreased in NCRR patients. Moreover, the ratio of phosphorylation pyruvate dehydrogenase reduced to near normal

Correspondence to: Shengshou Hu, MD, PhD or Jiangping Song, MD, PhD, Cardiomyopathy Research Group at Fuwai Hospital, State Key Laboratory of Cardiovascular Disease, National Center for Cardiovascular Diseases, Beilishi Rd No. 167, Beijing 100037, China. Email fwhushengshou@163.com, fwsongjiangping@126.com
*M. Xu, H. Zhang, and Y. Chang contributed equally.
Supplemental Material is available at https://www.ahajournals.org/doi/suppl/10.1161/CIRCHEARTFAILURE.123.011504.
For Sources of Funding and Disclosures, see page 696.

Circulation: Heart Failure is available at www.ahajournals.org/journal/circheartfailure

WHAT IS NEW?

- Single-nucleus transcriptional profiles of heart tissues from left ventricular assist device–supported patients with different outcomes were generated to dissect the cellular characteristics of cardiac reverse remodeling.
- A comparison of single-nucleus RNA sequencing data and animal experiments revealed that increased expression of *ATP5F1A* by cardiomyocytes promoted cardiac reverse remodeling.
- *ATP5F1A* exerted cardiac reverse remodeling by improving the heart function and morphology.

WHAT ARE THE CLINICAL IMPLICATIONS?

- The transverse aortic constriction and dilated cardiomyopathy model described herein could demonstrate that overexpression of *ATP5F1A* could inhibit the progression of heart failure and promote cardiac reverse remodeling, respectively.
- Cardiac reverse remodeling could be promoted by increasing the expression of *ATP5F1A* in cardiomyocytes.

Nonstandard Abbreviations and Acronyms

AAV9	adeno-associated virus 9
CRR	cardiac reverse remodeling
DCM	dilated cardiomyopathy
EC	endothelial cell
HF	heart failure
LVAD	left ventricular assist device
LVEDV	left ventricular end-diastolic volume
LVEF	left ventricular ejection fraction
MPC	mitochondrial pyruvate carrier
NC	normal control
NCRR	no cardiac reverse remodeling
OMIHC	opal multicolor immunohistochemical
snRNA-seq	single-nucleus RNA sequencing
TAC	transverse aortic constriction

after LVAD support in CRR patients but not in NCRR patients.[3]

Defining the specific cell types and their mechanisms that promote CRR could help in developing therapeutic targets. Myocardial tissue contains a variety of cells, and each cell type possesses a unique function.[4] Bulk RNA sequencing has clarified cell differences at an average level and cannot clarify differences in cell subtypes. Single-nucleus RNA sequencing (snRNA-seq) can clarify the heterogeneity of various cells (especially cardiomyocytes) at single-cell resolution.[5] In this study, we aimed to establish the single-cell landscape of CRR in LVAD-supported patients. Hopefully, this study will pave the way for the precision therapy of HF in the near future.

METHODS

The data and scripts/code that support the findings of this study are available from the corresponding author upon reasonable request.

Sample Collection

This study was approved by the Human Ethics Committee of Fuwai Hospital. All patients provided written informed consent. The LVAD samples were obtained from the LVAD cores at the time of implantation, following the methods of the previous study.[6] The identical regions from the normal control (NC) were obtained from donors, who were unsuitable for heart transplantation due to noncardiac reasons such as body-weight mismatch. Echocardiography was performed at the time of implantation and during follow-up. The post-LVAD echocardiographic parameters were recorded 30 minutes after adjusting the LVAD rotational speed to no forward blood flow in the pipeline. CRR was defined as those who met all the following criteria: postoperative (3-month) left ventricular ejection fraction (LVEF) ≥40%, postoperative (3-month) left ventricular end-diastolic dimension <6 cm, and an increase in LVEF ≥5% compared with preoperative LVEF. The process of snRNA-Seq is provided in the Supplemental Material.

Transverse Aortic Constriction and Dilated Cardiomyopathy Mouse Model

All animal experiments were approved by the Animal Ethics Committee of Fuwai Hospital. We used the ARRIVE (Animal Research Reporting of In Vivo Experiments) reporting guidelines.[7] Mice were fed a chow diet and housed in a barrier facility with 12-/12-hour light/dark cycles, a humidity of 50±3%, and a temperature of 25±2 °C. The aorta of a C57BL/6J mouse from the same cage was constricted by a 7-0 monofilament polypropylene suture paralleled with a 27-gauge needle. The details of the procedure were available in previous studies.[8] Because there was no significant difference in LVEF between female and male mice after transverse aortic constriction (TAC) surgery,[9] female and male mice with LVEF ≤50% 4 weeks after surgery were included. Dilated cardiomyopathy (DCM) mouse model was established by a $cTnT^{R141W}$ (cardiac troponin T) gene transgenic mouse model.[10] Similarly, there was no significant difference in LVEF between female and male DCM mice,[11] and female and male mice with LVEF≤50% were included.

Adeno-Associated Virus 9 Vector Construction and Injection

ATP5F1A fragment (NM_007505.2) was cloned into an AAV9 (adeno-associated virus 9) vector (pAV-U6-cTNT-flag) to construct AAV9-cTNT-*ATP5F1A*. The 3-week-old C57BL/6J mice and 15-week-old DCM mice were randomly assigned to be injected with either 1×10^{12} virus genome/mouse AAV9-cTNT-*ATP5F1A* or AAV9-cTNT-vehicle via tail vein.

Histopathologic Analysis

Samples were fixed with formaldehyde and embedded in paraffin, sectioned at 8 μm. Masson trichrome staining

(Solarbio, G1340) was performed to assess fibrosis. Opal multicolor immunohistochemical (OMIHC) staining was performed according to the protocol as previously described.[12] The antibodies used are given as follows: *ATP5F1A* (Abcam, ab176569) at 1:100, TTN (Abcam, ab307446) at 1:1000, CD68 (Abcam, ab955) at 1:1000, SPARC (Abcam, ab203284) at 1:500, *HSPG2* (Abcam, ab2501) at 1:200, CD31 (Abcam, ab182981) at 1:1000, LDB2 (Proteintech, 11873-1-AP) at 1:500, TXNIP (Abcam, ab188865) at 1:200, ACTC1 (Abcam, ab46805) at 1:200, MYH6 (Proteintech, 22281-1-AP) at 1:200, CD3 (Abcam, ab16669) at 1:150, CD2 (Abcam, ab314761) at 1:100, PTK2 (Abcam, ab40794) at 1:250, GNLY (Abcam, ab241333) at 1:1000, IL7R (Abcam, ab259806) at 1:500, vWF (Abcam, ab6994) at 1:300, FLRT2 (GeneTex, GTX123309) at 1:500, PCSK5 (Proteintech, 16470-1-AP) at 1:100, and PDE3A (Abcam, ab244337) at 1:500. The slides were analyzed using the Vectra Quantitative Pathology Imaging System (PerkinElmer). The histopathologic staining was quantified using Image J software, version 1.53 (ratio of the positive area to the total section area).

Echocardiography

Mice were anesthetized by 2% isoflurane and placed in the supine position. Transthoracic echocardiography was performed by using the Vevo 3100 Imaging System (FUJIFILM). Vevo LAB 3.0 software was utilized to analyze the LVEF and left ventricular end-diastolic volume (LVEDV). No data were excluded. The experienced analyst of the echocardiography was blinded to the groups. After the last echocardiography, the mice were euthanized in a CO_2 chamber.

Oxygen Consumption Rate and Extracellular Acidification Rate Calculation

The 100-μm heart tissue was put in the Islet Capture microplates (Agilent, 103518-100) and tested by the Seahorse XF Cell Mito Stress Test Kit (Agilent, 103015-100). The Seahorse XFe24 analyzer was performed according to the manufacturer's protocol.

Statistical Analysis

For non-snRNA-seq data, an unpaired, 2-tailed Student *t* test was used. All values were presented as mean±SD. $P<0.05$ was considered statistically significant.

RESULTS

Baseline and Follow-Up Characteristics of Patients Supported With LVAD

A total of 8 patients were enrolled in this study. During the follow-up, 4 patients showed persistent increased LVEF and decreased left ventricular end-diastolic dimension and were defined as CRR. The NT-proBNP of the CRR patient decreased from 3384±1679 to 461±238 pg/mL (Table S1; Figure S1). The baseline characteristics of CRR and NCRR patients at the time of LVAD implantation are shown in Table S2. There was no significant difference in baseline characteristics such as age, HF cause, and complications between the 2 groups.

Cell Types in NC, CRR, and NCRR Patients

Nuclei suspensions from 4 NC, 4 CRR, and 4 NCRR patients were subjected to snRNA-seq (Figure 1A). After performing quality control, we analyzed 126 156 nuclei (Figure S2A through S2C). We identified cardiomyocytes expressing *TTN*, fibroblasts expressing *DCN*, endothelial cells (ECs) expressing *vWF*, macrophage expressing *CD163*, lymphocytes expressing *SKAP1*, smooth muscle cells expressing *MYH11*, pericytes expressing *RGS5*, neurons expressing *NRXN1*, adipocytes expressing *GPAM*, and proliferating cells expressing *MKI67* (Figure 1B). The marker genes were visualized in each distinct cell type (Figure 1C). The independent distribution of marker genes for each cell type further confirmed the accuracy of the cell type assignment (Figure 1D). In addition, the uniform manifold approximation and projection distribution of each sample showed no significant batch effect (Figure S3). The proportion of cardiomyocytes was lower in patients with HF than in NC, while the proportion of cardiomyocytes was higher in CRR than in NCRR patients (Figure 1E). Overall, there were differences in the cellular composition of the 3 groups.

Identifying Difference of Cardiomyocyte in 3 Groups

About 25 690 cardiomyocytes were assembled into 4 clusters (Figure 2A). CM1 demonstrated high expression of *LDB2* (Figure 2B), which was associated with heart development.[13] In addition, CM1 expressed genes associated with muscle contraction and ATP metabolism (Figure S4A), including *GSN*[14] and *AKT3*.[15] CM2 expressed *TXNIP* (Figure 2B), which mediated oxidative stress under lactic acidosis.[16] CM2 expressed high level of *PDK4* that inhibited glucose metabolism leading to a decrease in energy production[3] (Figure S4A). Maladaptive markers for starvation and stress-responses genes, such as *ANKRD1*[17] and *PRKAA2*,[18] were increased in CM2 (Figure S4A). CM3 expressed *ACTC1*, *ADRA1A*, and *IDH2* (Figure 2B; Figure S4A), which participated in heart contraction.[19–21] CM4 demonstrated high expression of genes related to heart contraction, such as *MYH6*[22] and *CACNA1C*[23] (Figure 2B; Figure S4A). OMIHC confirmed the presence of the 4 cardiomyocyte clusters (Figure S4B). We further analyzed the proportion and functional differences between the 4 clusters of cardiomyocytes. CM1 was higher in NC than in the other 2 groups. CM2 was almost present in patients with HF. CM3 and CM4 were also predominantly distributed in NC (Figure 2C). Gene ontology enrichment analysis showed that CM1 mainly functioned in myofilament contraction–related processes. CM2 participated in the

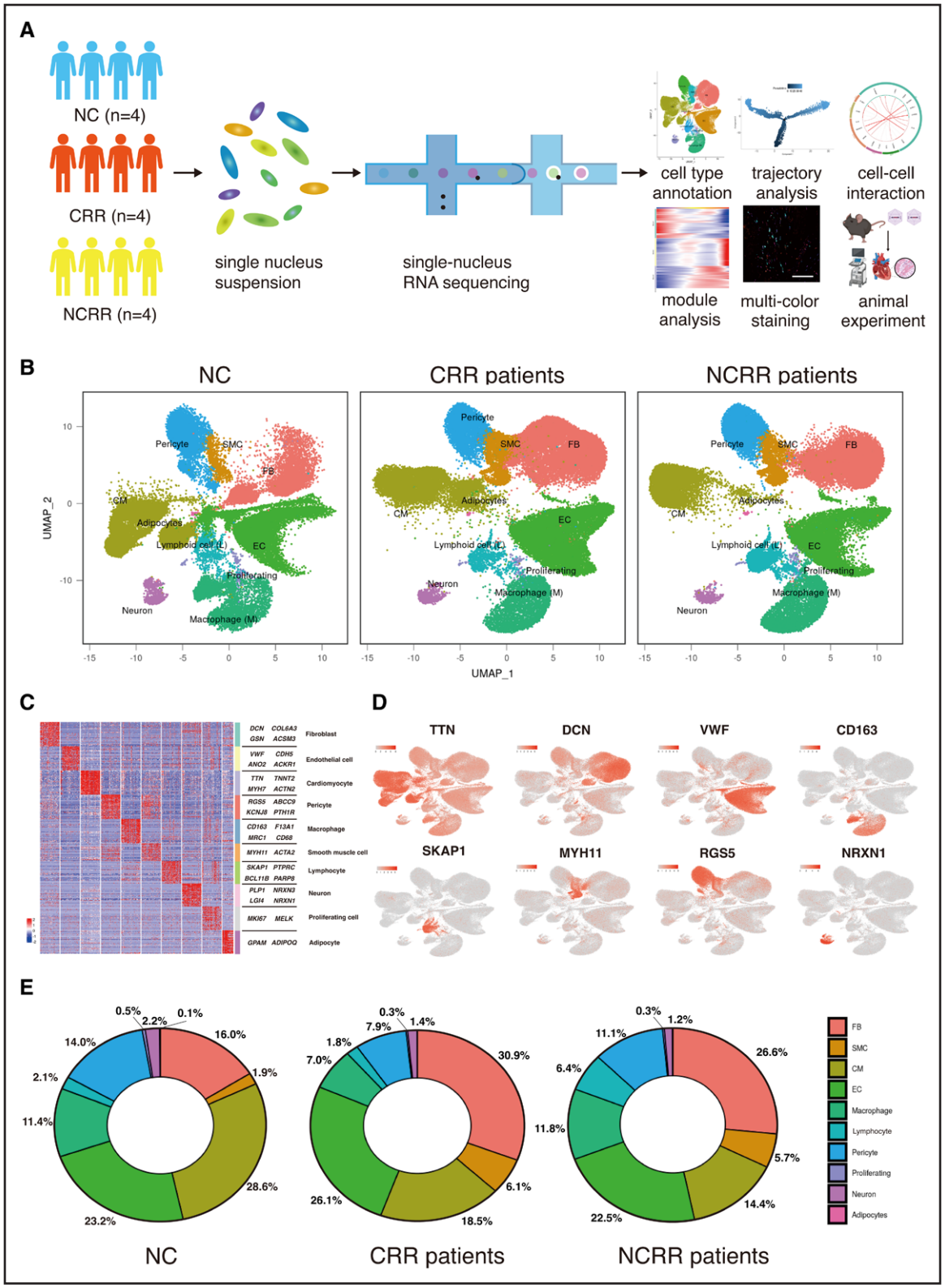

Figure 1. Overview of the 126 156 single nuclei from normal control hearts and left ventricular assist device–supported patients. **A**, Flowchart and data analysis strategy (n=4 for normal control [NC], n=4 for cardiac reverse remodeling [CRR], and n=4 for no cardiac reverse remodeling [NCRR]). **B**, Profiles of the uniform manifold approximation and projection plots of the 126 156 nuclei. **C**, Heatmap showing the differentially expressed genes of each cell type. The selected marker genes for each cell type are highlighted. **D**, Expression of marker genes in each cell type. **E**, Plots showing the fraction of each cell type in the 3 different groups.

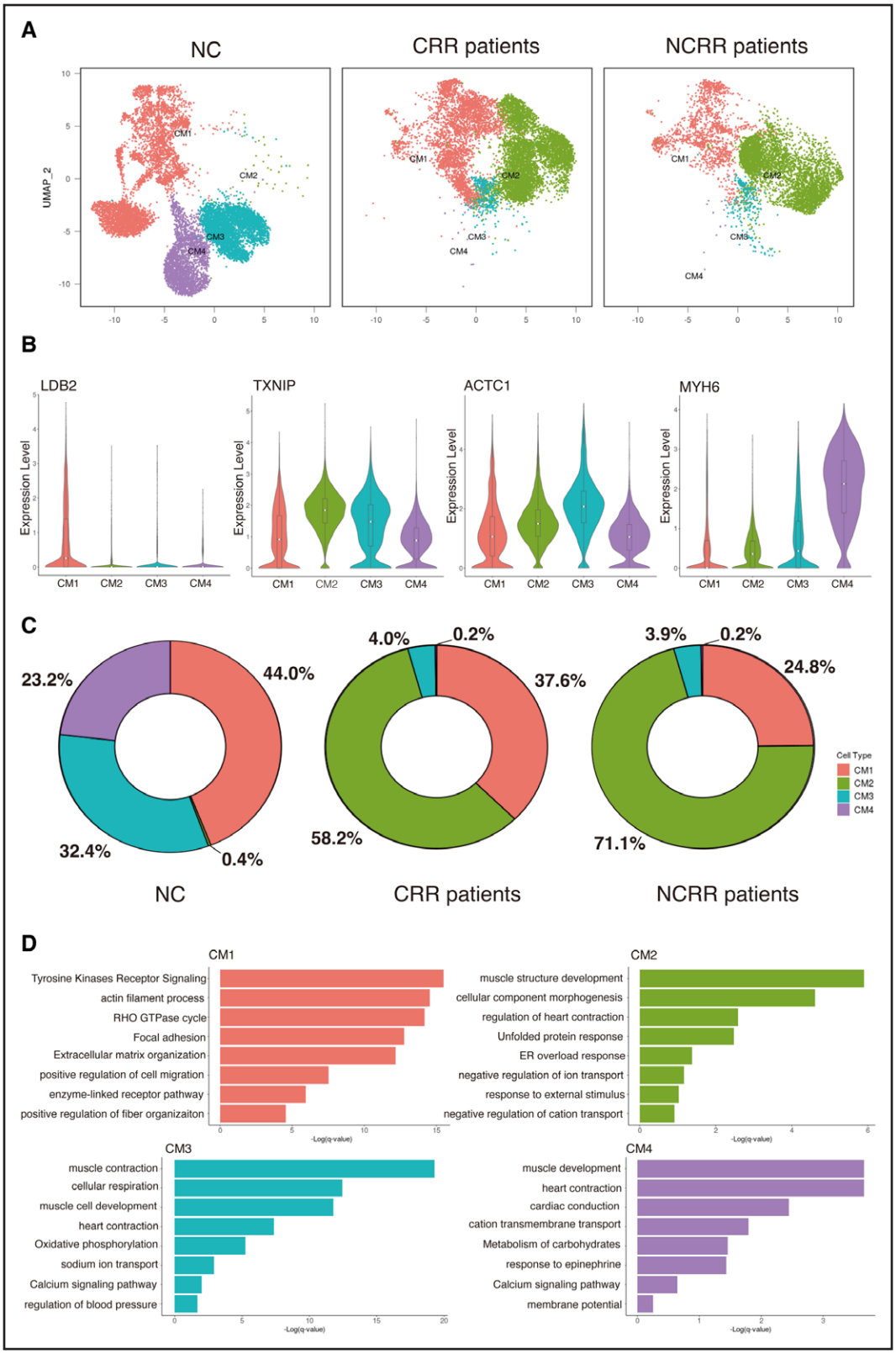

Figure 2. Cardiomyocyte (CM) cluster.
A, The uniform manifold approximation and projection plots of 25 690 CMs color coded by cluster. **B**, Violin plots showing the expression of specific marker genes in each CM cluster. **C**, Plots showing the difference in the proportion of CMs between the 3 groups. **D**, Bar plot showing the functional analysis of different CM clusters. CRR indicates cardiac reverse remodeling, n=4; NC, normal control, n=4; and NCRR, no cardiac reverse remodeling, n=4.

endoplasmic reticulum overload response and unfolded protein response. CM3 and CM4 were involved in cardiomyocyte contraction–related pathways (Figure 2D). Gene ontology enrichment analysis indicated that CM2 might be under stress and have impaired contractile function (Figure 2D). CM2 was significantly increased in patients with HF (Figure S4C). These changes might lead to a decrease in cardiac function.

Cardiomyocytes in CRR Patients Showed Enhanced ATP Anabolism

CRR patients had more CM1 than NCRR patients (Figure 3A). CM1 in CRR patients showed increased expression of ATP synthesis–related genes such as *ATP5F1A*[24] (Figure 3B). The function of ATP synthesis and cardiac muscle contraction were significantly higher in the CRR patients than in the other 2 groups (Figure 3C). OMIHC showed that cardiomyocytes in CRR patients expressed more *ATP5F1A* than the NCRR patients ($P<0.0001$; Figure 3D). *ATP5F1A* was significantly correlated to the LVEF of post-LVAD ($R^2=0.8501$; $P=0.0011$; Figure 3D). It suggested that enhanced ATP anabolism by cardiomyocytes was an important feature of CRR.

We performed a pseudotime analysis and obtained a proposed time-series trajectory containing 4 cardiomyocyte clusters (Figure 3E). Notably, cardiomyocytes in the NC were mainly distributed at the initial position of the pseudotime trajectory, while cardiomyocytes in the CRR and NCRR patients were mainly distributed at the 2 terminal positions. We quantified the proportion of each state in the 3 groups. The proportion of state 3 increased in CRR patients. The genes highly expressed in state 3 were mainly involved in heart contraction (Figure 3F). Based on the characteristics of gene expression during the pseudotime trajectory, it could be divided into 3 modules (Figure 3G). As genes in module1 were highly expressed early in the pseudotime trajectory, these genes might promote CRR. Further analysis of genes in module1 showed that genes involved in Ca^{2+} transport proteins (*CACNA1C*, *RYR*) and myocardial contractile proteins (*TNNT2*, *TNN*) decreased as the pseudotime progressed (Figure 3H). The previous study showed that a slower increase of Ca^{2+} concentration in cardiomyocytes inhibited CRR.[6]

Identifying Difference of Macrophages in 3 Groups

About 12 486 macrophages were divided into 5 clusters (Figure 4A). Macrophage1 expressed high levels of *LYVE1*, macrophage2 expressed a high level of *MERTK*, and macrophage4 expressed a high level of *RUNX1T1* (Figure S5A). The above genes were related to tissue-resident macrophage.[25–27] Macrophage3 expressed a high level of *ITGAX* (Figure S5A), thus denoted a subset of proinflammatory macrophage.[28] *HLA-DRA*, which marked antigen-presenting cells, was found in macrophage5 (Figure S5A). In addition, macrophage1 expressed *FGF13* (Figure 4B), which might be involved in regulating cardiac Na^+ currents.[29] Macrophage2 overexpressed *ZBTB16* (Figure 4B), which inhibited gene expression.[30] Macrophage3 overexpressed *DOCK10* (Figure 4B), which enhanced the inflammatory function of macrophage.[31] Macrophage4 expressed *DLC1* (Figure 4B), which suppressed inflammatory gene expression.[32] Macrophage5 expressed high level of *RPS27A* (Figure 4B).

Macrophage1 was predominantly distributed among NCRR patients (Figure 4C). In contrast, macrophage2 was predominantly distributed in NC and CRR patients (Figure 4C). The distribution of macrophage3 was similar to macrophage1 (Figure 4C). Macrophage4 was slightly higher in the NC and CRR patients than in the NCRR patients (Figure 4C). Macrophage5 was only present in NCRR patients (Figure 4C). Gene ontology enrichment analysis showed that macrophage1 mainly functioned in the immune response pathway. Macrophage2 was associated with myofilament sliding–related processes. Macrophage3 mainly functioned in leukocyte activation. Macrophage4 mainly participated in vascular development. Macrophage5 was mainly associated with antigen presentation (Figure 4D).

Macrophages in CRR Patients Were Correlated With Angiogenesis

The proportion of macrophage2 and macrophage4 was higher in CRR patients than those in NCRR patients (Figure 5A and 5B). In CRR patients, macrophage2 expressed a high level of *SPARC*, an anti-inflammatory[33] and angiogenesis regulator,[34] and macrophage4 expressed a high level of *HSPG2*, a gene that inhibited the inflammatory response.[27] OMIHC confirmed the results of snRNA-seq (Figure 5C and 5D).

Pseudotime analysis showed that the initial position of the trajectory was mainly the macrophages from NC, while macrophages in the CRR and NCRR patients were mainly distributed in the 2 terminal positions (Figure 5E). The characteristics of gene expression could be divided into 3 modules (Figure 5F). Genes in module2 were mainly expressed at the beginning of the trajectory and genes involved in angiogenesis (*PDGFRA* and *EGFR*) and anti-inflammatory response (*HSPG2*, *ZEB1*, and *RUNX1T1*) decreased as the trajectory progressed (Figure 5G). OMIHC showed that SPARC and HSPG2 were positively correlated with CD31 in CRR patients (Figure 5C and 5D). These suggested that macrophages exerting anti-inflammatory function and promoting angiogenesis were important features of CRR.

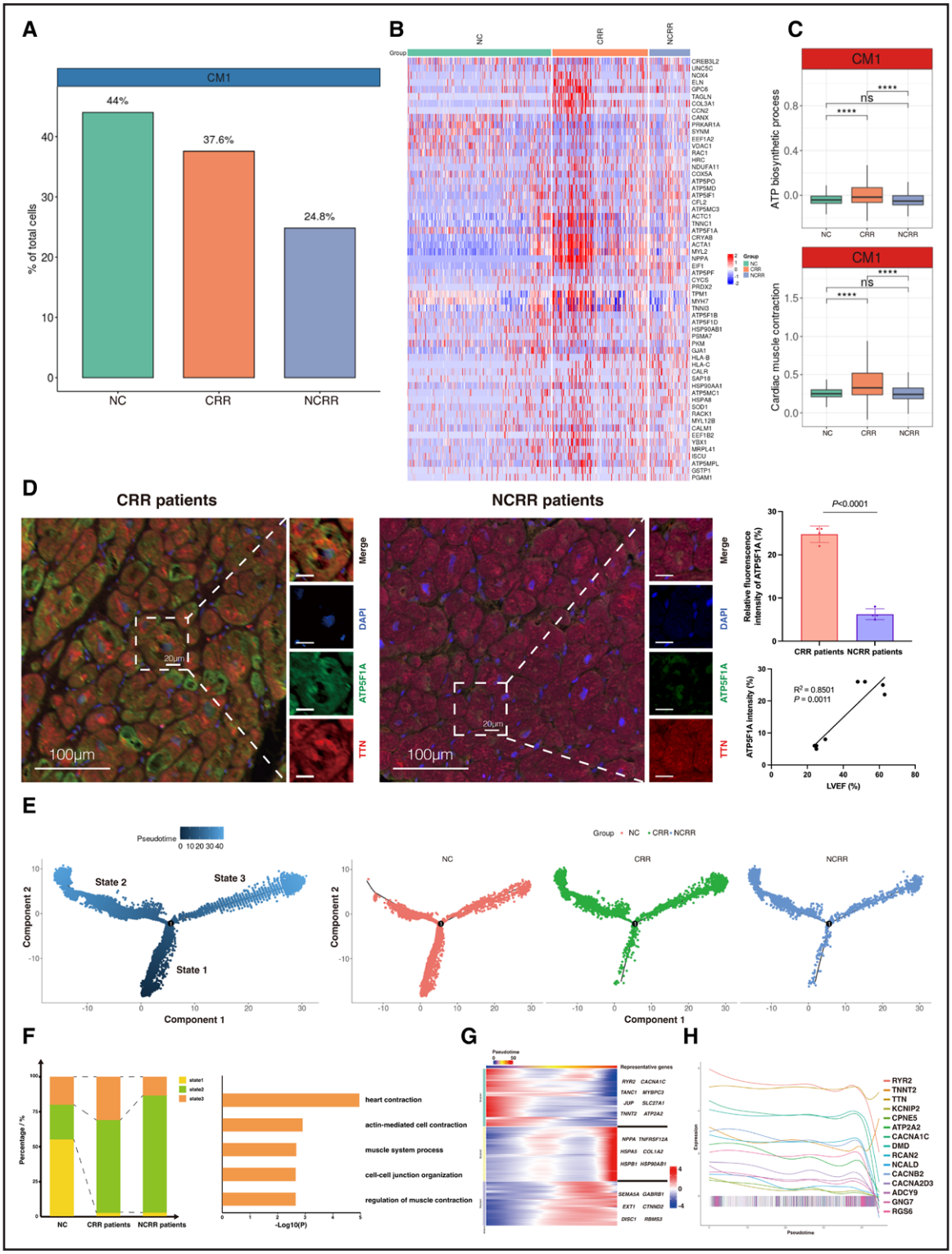

Figure 3. Analysis of differences between groups and pseudotime analysis of cardiomyocyte (CM).
A, Differences in the proportion of CM1 in the 3 groups. **B**, Heatmap of expression of ATP anabolic genes and myocardial contraction genes in the 3 groups. **C**, Functional scores of ATP biosynthetic process and cardiac muscle contraction in the 3 groups. **D**, Opal multicolor immunohistochemical staining for *ATP5F1A* in CM (TTN; n=4 for cardiac reverse remodeling [CRR] and n=4 for no cardiac reverse remodeling [NCRR]; data are expressed as mean±SD). **E**, CM pseudotime analysis. **F**, Bar plot showing the proportion of the state 1 to state 3 CMs and the main function of state 1 CM. **G**, Trajectory module analysis of CM. **H**, Myocardial contraction gene and Ca^{2+} transmembrane transporter gene expression along the pseudotime trajectory. NC indicates normal control.

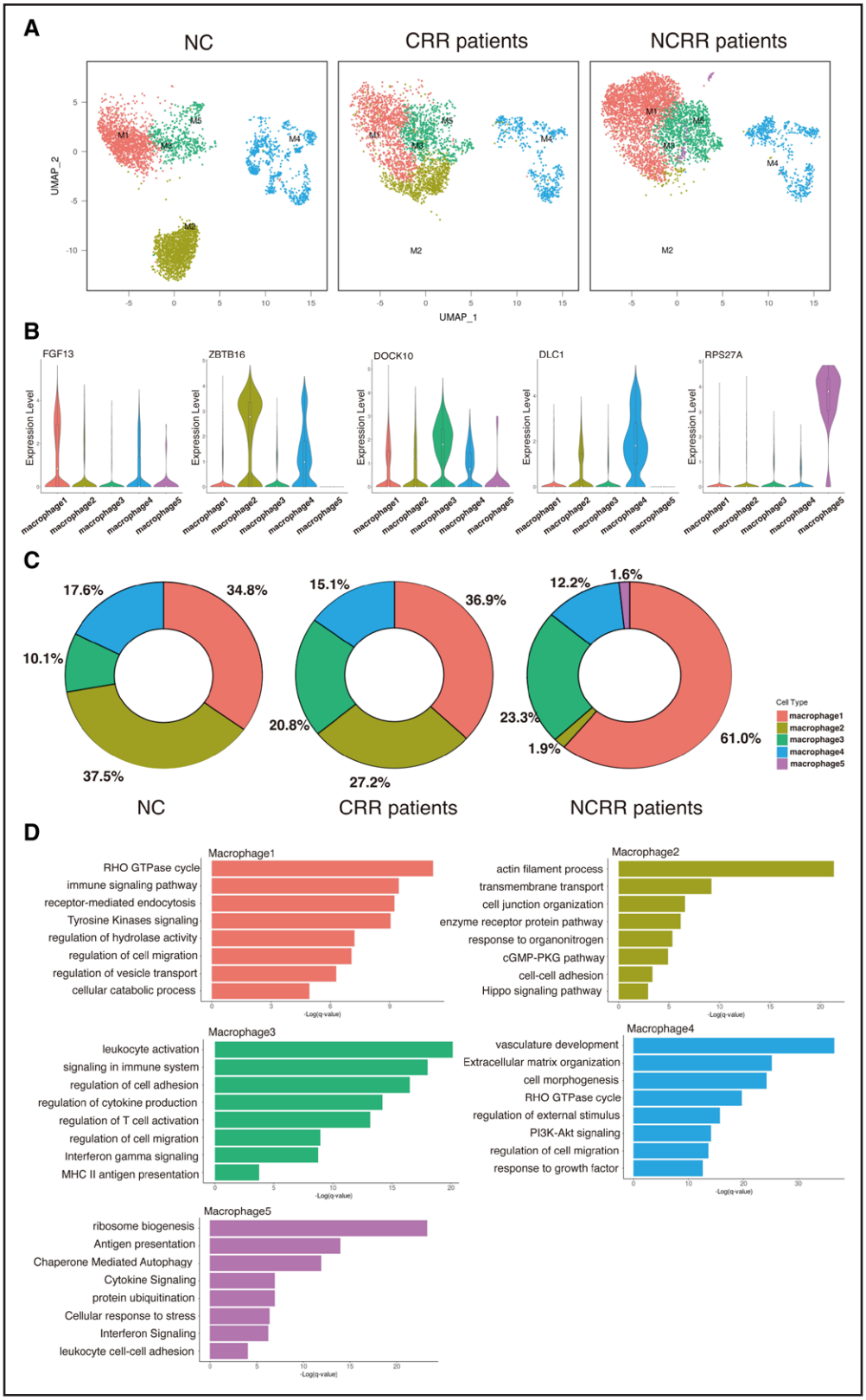

Figure 4. Macrophage cluster.
A, The uniform manifold approximation and projection plots of 12 486 macrophages color coded by cluster. **B**, Violin plots showing the expression of specific marker genes in each macrophage cluster. **C**, Plot showing the difference in the proportion of macrophages between the 3 groups. **D**, Bar plot showing the functional analysis of different macrophage clusters. CRR indicates cardiac reverse remodeling, n=4; NC, normal control, n=4; and NCRR, no cardiac reverse remodeling, n=4.

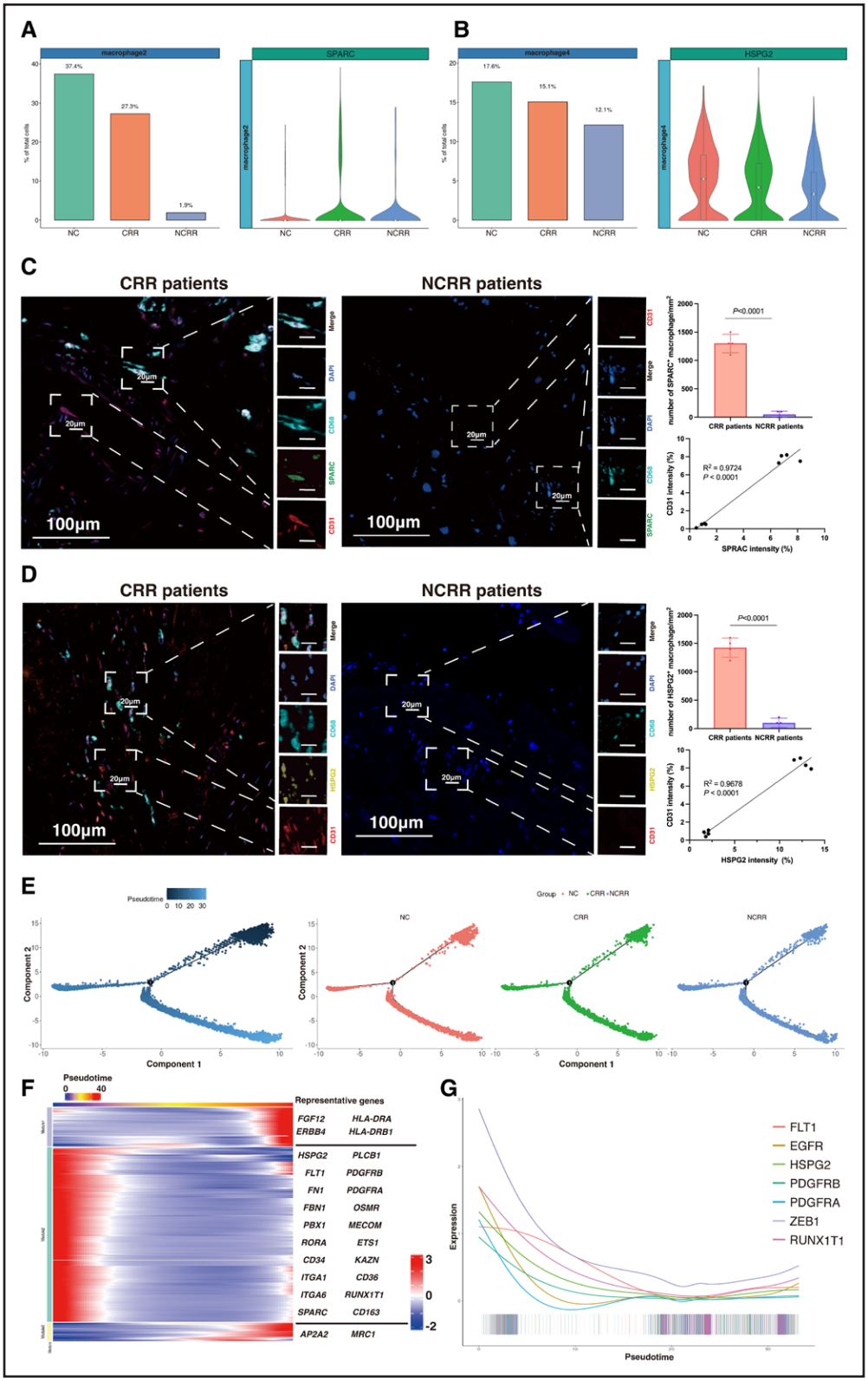

Figure 5. Analysis of differences between groups and pseudotime analysis of macrophage.
A, Differences in the proportion of macrophage2 in the 3 groups. **B**, Differences in the proportion of macrophage4 in the 3 groups. **C**, Opal multicolor immunohistochemical staining for SPARC, CD68, and CD31 (n=4 for cardiac reverse remodeling [CRR] and n=4 for no cardiac reverse remodeling [NCRR]; data are expressed as mean±SD). **D**, Opal multicolor immunohistochemical staining for HSPG2, CD68, and CD31 (n=4 for CRR and n=4 for NCRR; data are expressed as mean±SD). **E**, Macrophages pseudotime analysis. **F**, Trajectory module analysis of macrophages. **G**, Anti-inflammatory gene expression and promoting angiogenesis gene expression along the pseudotime trajectory. NC indicates normal control.

Lymphocytes in CRR Patients Showed Increased Proangiogenic Effect

About 4217 lymphocytes were assembled into 4 clusters (Figure S6A). Lymphocyte1 expressed genes associated with T-cell activation, such as *CD2* and *CD69* (Figures S6B and S7A). Lymphocyte2 expressed *PTK2*, *FLT1*, and *PDE7B* (Figures S6B and S7A), representing proangiogenic T cells.[35] Lymphocyte3 expressed *GNLY* and *GZMB* (Figures S6B and S7A), representing cytotoxic T cell.[36] Lymphocyte4 expressed a high level of *IL7R* (Figure S6B), which was associated with long-term immune memory.[17] CRR patients possessed more lymphocyte4 than the NCRR patients (Figure S6C). OMIHC confirmed the shifts in cell composition of the 4 lymphocyte clusters (Figure S7B). Gene ontology enrichment analysis showed that lymphocyte4 functioned in the VEGFA-VEGFR2 signaling pathway (Figure S6D).

EC-Immune Cell Interactions Promoted Angiogenesis

EC was divided into 4 clusters (Figure 6A). Based on the established markers[5,17] (Figure S8A), the EC was assigned to capillary EC (EC1 marked by *RGCC*) and arterial EC (EC2, EC3, and EC4, marked by *NPR3*, *SEMA3G*, and *PRKG1* respectively). In addition, EC1 expressed *CD36* (Figure 6B), which was associated with angiogenesis.[37] EC2 demonstrated high expression of *FLRT2* (Figure 6B), which promoted proliferation.[38] *PCSK5* was differentially expressed in EC3 (Figure 6B), which participated in keeping the morphogenesis of the vessel.[39] EC4 highly expressed *PDE3A* (Figure 6B), which regulated EC permeability.[40] EC1 and EC4 were mainly present in NC (Figure 6C). EC2 and EC3 were mainly present in CRR and NCRR patients, respectively (Figure 6C). All EC clusters possessed angiogenic capacity, but EC3, which was more abundant in the NCRR patients, was further involved in the inflammatory response (Figure 6D). OMIHC confirmed the composition shifts in cell composition (Figure S8B).

As macrophage2 expressed a high level of *SPARC*, an angiogenesis regulator, macrophage4 and lymphocyte2 functioned in angiogenesis. We analyzed the intercellular interactions between ECs and immune cells that were elevated in CRR patients (macrophage2, macrophage4, and lymphocyte2). The top 10 intercellular interactions showed that immune cells interacted with EC mainly through THBS1 (thrombospondin-1)-CD36, VEGF-FLT1 (vascular endothelial growth factor-fms-like tyrosine kinase 1), and CD74-APP (amyloid-β precursor protein) (Figure 6E).

Overexpression of *ATP5F1A* in Cardiomyocytes Could Promote CRR

TAC and DCM mice were used to investigate the effect of overexpressing *ATP5F1A* on CRR (Figure 7A). C57BL/6J mice received AAV9 injections 2 weeks before TAC surgery. Echocardiography was performed at 42 and 56 days after injection. In mice treated with AAV9-cTNT-ATP5F1A, LVEF was significantly higher and LVEDV was significantly lower at 56 days after injection than those at 42 days after injection (LVEF: 42 versus 56 days=43.8±4.4% versus 82.0±2.6%; P=0.0002; LVEDV: 42 versus 56 days=56.3±0.5 versus 45.9±3.6 μL; P=0.0075). In untreated and AAV9-cTNT-vehicle–treated TAC mice, LVEF was significantly lower at 56 days after injection than that at 42 days after injection (untreated LVEF: 42 versus 56 days=44.1±2.8% versus 37.8±0.2%; P=0.0178; vehicle-treated LVEF: 42 versus 56 days=42.7±1.0% versus 36.7±1.4%; P=0.0037). The LVEDV of AAV9-cTNT-vehicle–treated TAC mice was significantly higher at 56 days after injection than at 42 days after injection (42 versus 56 days=63.1±5.9 versus 77.6±5.7 μL; P=0.0378). Compared with 42 days after injection, *ATP5F1A* expression at 56 days after injection in AAV9-cTNT-*ATP5F1A*–treated mice was significantly higher (42 versus 56 days=9.8±1.3% versus 51.5±4.6%; P<0.0001) but not in AAV9-cTNT-vehicle–treated mice (42 versus 56 days=9.5±2.4% versus 10.7±1.8%; P=0.0606; Figure S9A). The above results indicated that overexpression of *ATP5F1A* inhibited HF progression. Moreover, the AAV9 was only enriched in the heart (Figure S9B). These results indicated that the AAV9-cTNT-*ATP5F1A* was specific to cardiomyocytes and possessed high efficacy.

For DCM mice, echocardiography was performed at preinjection and 56 days after injection. In DCM mice treated with AAV9-cTNT-*ATP5F1A*, LVEF was significantly higher and LVEDV was significantly lower at 56 days after injection than those at preinjection (LVEF: preinjection versus 56 days=31.5±0.8% versus 62.0±4.8%; P=0.0004; LVEDV: preinjection versus 56 days=99.7±6.0 versus 68.6±10.7 μL; P=0.0116). In untreated and AAV9-cTNT-vehicle–treated DCM mice, LVEF was significantly lower and LVEDV was significantly higher at 56 days after injection than those at preinjection (untreated LVEF: preinjection versus 56 days=29.9±2.1% versus 23.5±2.5%; P=0.0261; vehicle-treated LVEF: preinjection versus 56 days=33.0±2.6% versus 27.6±1.9%; P=0.0410; untreated LVEDV: preinjection versus 56 days=91.5±12.4 versus 123.0±14.7 μL; P=0.0470; and vehicle-treated LVEDV: preinjection versus 56 days=90.9±8.2 versus 113.4±10.2 μL; P=0.0416). Compared with preinjection, *ATP5F1A* expression at 56 days after injection in AAV9-cTNT-*ATP5F1A*–treated mice was significantly higher (preinjection versus 56 days=10.5±0.8% versus 41.2±1.7%; P=0.0001) but not in AAV9-cTNT-vehicle–treated mice (preinjection versus 56 days=12.1±0.6% versus 10.3±1.1%; P=0.5318; Figure S9A). The above results indicated that overexpression of *ATP5F1A* promotes CRR.

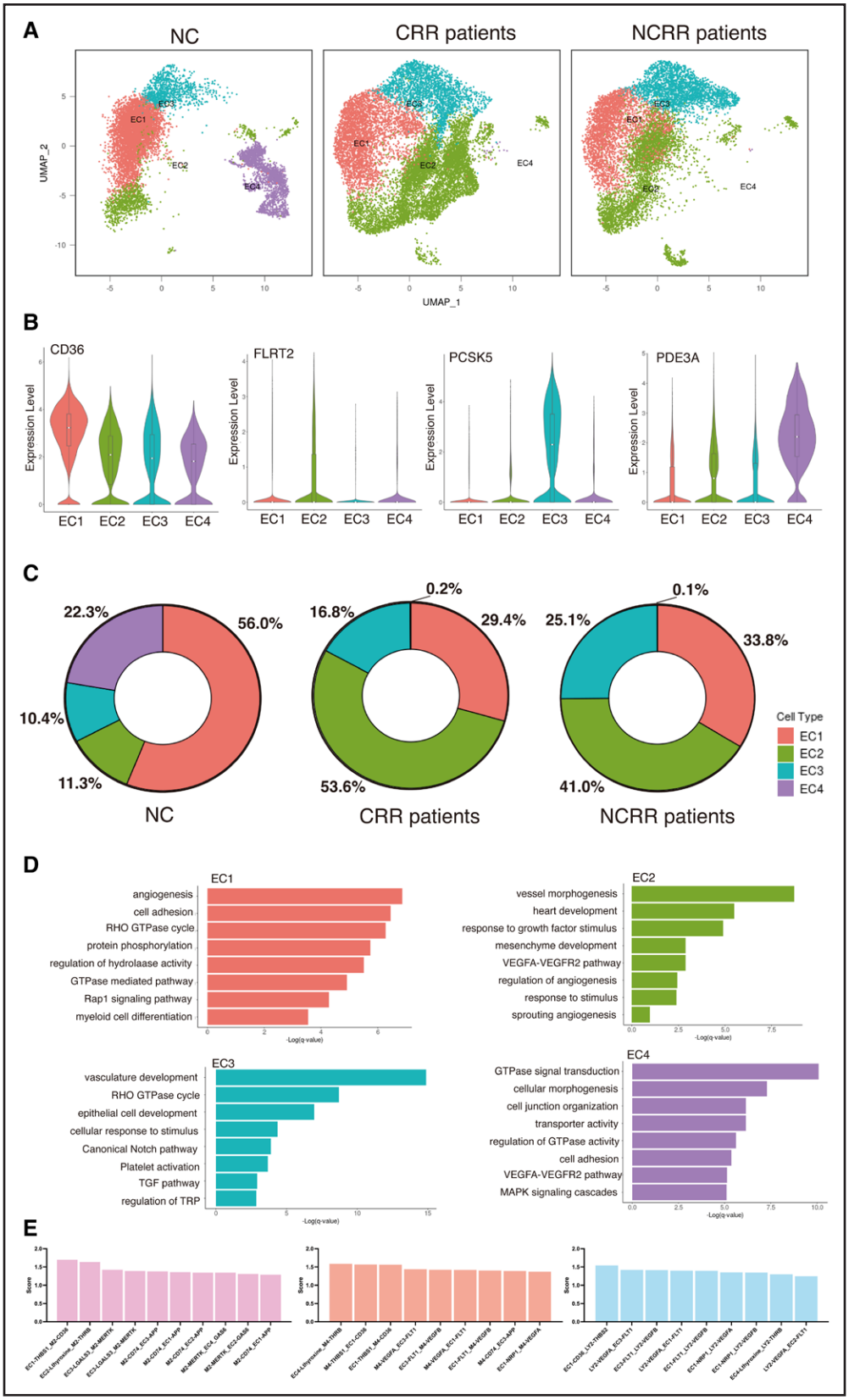

Figure 6. Endothelial cell (EC) cluster.
A, The uniform manifold approximation and projection plots of 30 359 ECs color coded by cluster. **B**, Violin plots showing the expression of specific marker genes in each EC cluster. **C**, Plot showing the difference in the proportion of ECs between the 3 groups. **D**, Bar plot showing the functional analysis of different EC clusters. **E**, Analysis of intercellular interactions of macrophage2, macrophage4, and lymphocyte2 with EC. CRR indicates cardiac reverse remodeling, n=4; NC: normal control, n=4; and NCRR, no cardiac reverse remodeling, n=4.

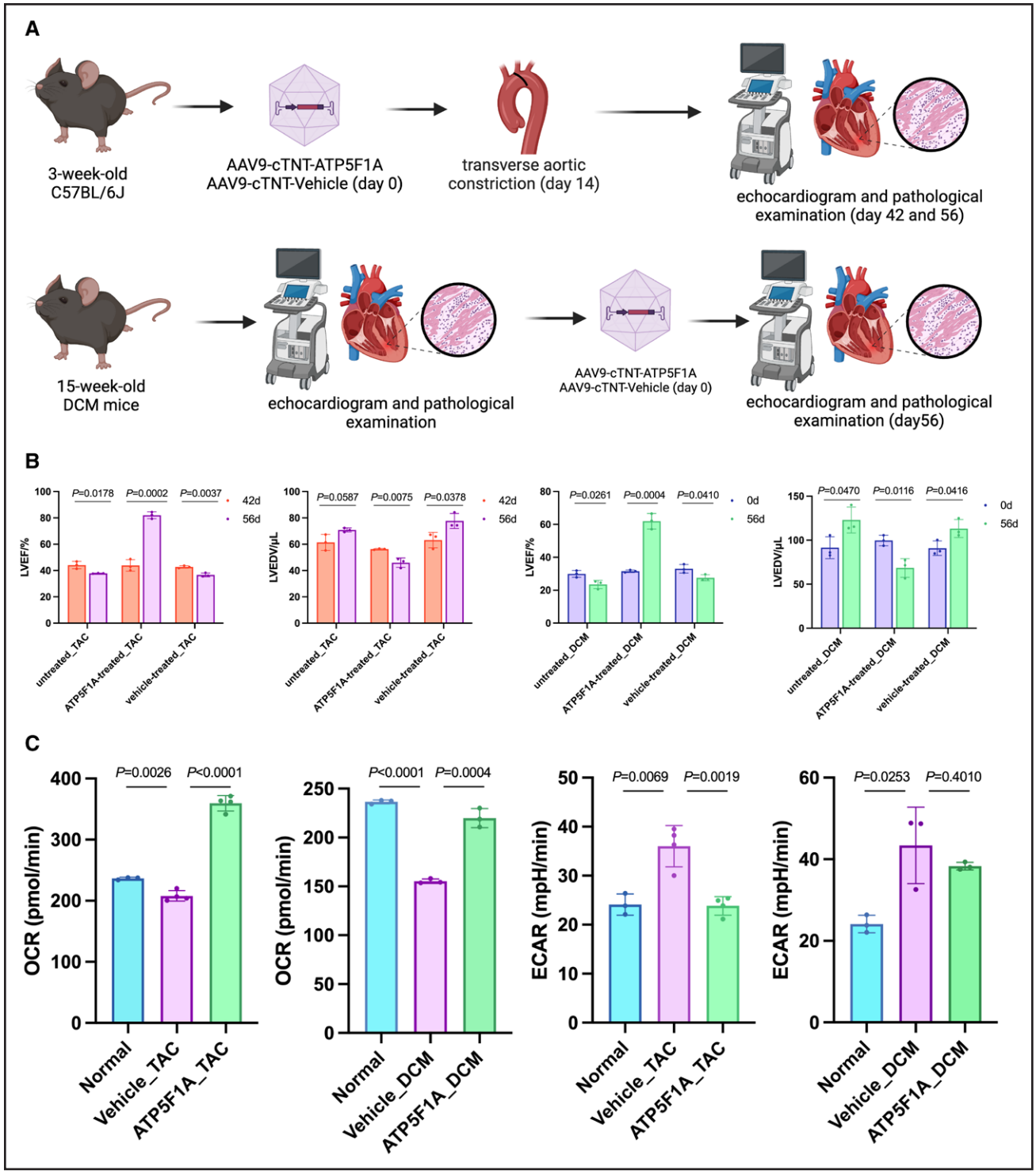

Figure 7. Overexpressing of *ATP5F1A* promotes cardiac reverse remodeling.
A, Workflow for in vivo AAV9-cTNT-*ATP5F1A* overexpressing experiments. **B**, Ultrasonographic examination of the left ventricular ejection fraction (LVEF) and left ventricular end-diastolic volume (LVEDV) in transverse aortic constriction (TAC) mice and dilated cardiomyopathy (DCM) mice. n=3 for each group. Data are expressed as mean±SD. **C**, The oxygen consumption rate (OCR) and extracellular acidification rate (ECAR) in DCM and TAC mice. n=3 for normal control, n=4 for TAC mice treated by AAV9-cTNT-vehicle, n=4 for TAC mice treated by AAV9-cTNT-*ATP5F1A*, n=3 for DCM mice treated by AAV9-cTNT-vehicle, and n=3 for DCM mice treated by AAV9-cTNT-*ATP5F1A*. Data are expressed as mean±SD. AAV9 indicates adeno-associated virus 9; and cTNT, cardiac troponin T.

We further evaluated the fibrosis and cell size by Masson and WGA staining, respectively. The degree of fibrosis and cell size in both TAC and DCM mice treated with AAV9-cTNT-*ATP5F1A* were significantly reduced at 56 days after injection (fibrosis in TAC: P=0.0018; fibrosis in DCM: P<0.0001; cell size in TAC: P=0.0002; and cell size in DCM: P=0.0001; Figure S9C and S9D). The above suggested that *ATP5F1A* was closely associated with the improvement of morphology and function. Moreover, we calculated the oxygen consumption rate to evaluate the level of oxidative phosphorylation. The results showed that the AAV9-cTNT-*ATP5F1A* significantly increased the oxygen consumption rate of TAC and DCM mice (359.5±12.6 pmol/min in TAC mice and 219.9±9.8 pmol/min in DCM mice) compared with that in vehicle mice (207.9±8.6 pmol/min in TAC vehicle mice; P<0.0001; 155.3±2.3 pmol/min in DCM vehicle mice; P=0.0004; Figure 7C). To further investigate glycolysis, we evaluated the extracellular acidification rate. AAV9-cTNT-*ATP5F1A* significantly reduced the extracellular acidification rate of TAC mice (23.8±1.9 mPH/min in TAC mice) compared with that in vehicle mice (36.0±4.2 mPH/min in TAC vehicle mice; P=0.0019; Figure 7C). There was no significant difference in the extracellular acidification rate between the DCM mice injected with AAV9-cTNT-*ATP5F1A* and the vehicle (Figure 7C). These results suggested that the overexpressing *ATP5F1A* in cardiomyocytes could enhance the function of mitochondria.

DISCUSSION

In this study, we systematically characterized the cellular composition of CRR at the single-cell resolution. In addition, we provided insight into the composition and functional alterations of cardiomyocytes, macrophages, lymphocytes, and EC, respectively. Several targets mediating CRR after LVAD support were also identified.

Cardiomyocytes were the main cell population that maintained the pumping function of the heart. Therefore, clarifying the characteristics of cardiomyocytes in CRR patients could provide new therapeutic insights into HF.

In this study, we found increased expression of ATP synthesis and metabolism genes (*ATP5F1A*) in cardiomyocytes of CRR patients. Previous findings showed a remodeling of energy metabolism in patients with HF, with a switch in the main metabolic substrate from fatty acids to glucose.[41] However, it was not clear the difference in metabolic characteristics of patients with different outcomes after LVAD support. Our results showed that the energy metabolism of cardiomyocytes was more efficient in CRR patients. The above results suggested that during HF in a subgroup of patients, cardiomyocytes compensated for the increased ATP synthesis capacity, and the above feature could promote the occurrence of CRR after LVAD support. In addition, HF mice overexpressing *ATP5F1A* showed improved function and morphology of the heart. The function of mitochondria was also elevated. On the contrary, the level of glycolysis did not show an increasing trend. It was reported that the glucose metabolism was enhanced in the rodent HF animal model.[42] Our results showed that *ATP5F1A* could induce the CRR by increasing ATP synthesis of mitochondria.

A small number of immune cells were involved in maintaining a normal cardiac microenvironment.[17] We identified 12 486 macrophages and 4217 lymphocytes. CRR patients possessed more macrophage2 and macrophage4 than NCRR patients. Both macrophage2 and macrophage4 expressed anti-inflammatory genes (macrophage2 expressed *SPARC* and macrophage4 expressed *HSPG2*) and showed proangiogenic effect. On the contrary, the main macrophage cluster within NCRR patients was macrophage1, whose functions were mainly involved in immune signaling pathways. This phenomenon revealed that the suppression of inflammatory response in patients could promote CRR. Regarding lymphocytes, no previous studies reported on its mediation of CRR. Our study divided lymphocytes into 4 clusters, where CRR patients possessed more lymphocyte2 than the other 2 groups and lymphocyte2 functioned in vascular development. The above results suggested that the angiogenic response was an important feature of CRR patients. Intercellular interaction analysis revealed that immune cells interacted with EC mainly through THBS1-CD36, CD74-APP, and VEGF-FLT1. All these receptor-ligand pairs possessed a strong proangiogenic function. Stimulation of luteal cells with prostaglandin F2α increased both *THBS1* and *CD36* expression, thereby promoting luteal angiogenesis.[43] In addition, *CD74* expression was increased in lung cancer tissues, accompanied by angiogenesis. When treated with anti-CD74 monoclonal antibody, the proangiogenic effect of CD74 was significantly inhibited. Administration of macrophage migration inhibitory factor resulted in increased *CD74* expression.[44] FLT1 was a receptor tyrosine kinase that bound to VEGF and played an important role in vascular development and angiogenesis.[45] The above findings might serve as targets for intervention to increase angiogenesis and promote CRR.

Our study has several limitations. The first is a small population of study patients. Due to the low incidence of CRR, we are unable to include more patients with CRR in the short term. At present, the application of LVAD in the treatment of end-stage HF is increasing, and more patients with CRR will be included in our research in the future. Second, the integration of NC samples is not good, resulting in cardiomyocytes being affected by a certain sample (NC1). Considering the animal experiments, the small sample size limits the robustness and rigor of the data despite the small within-group differences. We will

further investigate the mechanisms of overexpressing *ATP5F1A* on CRR in a larger data set and validate the conclusions in more animal models.

CONCLUSIONS

This study found that increased synthesis of ATP mediated by *ATP5F1A* was able to enhance contraction and promote CRR. Immune cells were also found to increase angiogenesis by interacting with EC, which also promoted CRR. This study provided robust evidence for screening CRR patients after LVAD support and offered a direction for validating the mechanism of CRR.

ARTICLE INFORMATION

Received December 19, 2023; accepted May 24, 2024.

Affiliations

Shenzhen Key Laboratory of Cardiovascular Disease, Fuwai Hospital Chinese Academy of Medical Sciences, China. Beijing Key Laboratory of Preclinical Research and Evaluation for Cardiovascular Implant Materials, Animal Experimental Centre, Fuwai Hospital, Chinese Academy of Medical Sciences and Peking Union Medical College, China. The Cardiomyopathy Research Group at Fuwai Hospital, State Key Laboratory of Cardiovascular Disease, National Center for Cardiovascular Diseases, Beijing, China.

Acknowledgments

Drs Xu, Zhang, and Hua isolated nuclei for single-nucleus RNA sequencing (snRNA-seq) analysis. Dr Chang, Y. Sheng, D. Shan, and M. Bao contributed to the RNA library preparation for the snRNA-seq. Drs Xu and Hua and X. Chen contributed to the analysis of the snRNA-seq and the article preparation. Drs Hu and Song designed the project, supervised the experiments, and reviewed the article.

Sources of Funding

This work was supported by the National Natural Science Fund for Distinguished Young Scholars of China (grant 82125004) and the Program for Guangdong Introducing Innovative and Entrepreneurial Teams (grant 2019ZT08Y481).

Disclosures

None.

Supplemental Material

Supplemental Methods
Tables S1 and S2
Figures S1–S9
Reference 46

REFERENCES

1. Roger VL. Epidemiology of heart failure. *Circ Res*. 2013;113:646–659. doi: 10.1161/CIRCRESAHA.113.300268
2. Bajpai G, Schneider C, Wong N, Bredemeyer A, Hulsmans M, Nahrendorf M, Epelman S, Kreisel D, Liu Y, Itoh A, et al. The human heart contains distinct macrophage subsets with divergent origins and functions. *Nat Med*. 2018;24:1234–1245. doi: 10.1038/s41591-018-0059-x
3. Cluntun AA, Badolia R, Lettlova S, Parnell KM, Shankar TS, Diakos NA, Olson KA, Taleb I, Tatum SM, Berg JA, et al. The pyruvate-lactate axis modulates cardiac hypertrophy and heart failure. *Cell Metab*. 2021;33:629–648.e10. doi: 10.1016/j.cmet.2020.12.003
4. Chaffin M, Papangeli I, Simonson B, Akkad A-D, Hill MC, Arduini A, Fleming SJ, Melanson M, Hayat S, Kost-Alimova M, et al. Single-nucleus profiling of human dilated and hypertrophic cardiomyopathy. *Nature*. 2022;608:174–180. doi: 10.1038/s41586-022-04817-8
5. Tucker NR, Chaffin M, Fleming SJ, Hall AW, Parsons VA, Bedi KC, Akkad A-D, Herndon CN, Arduini A, Papangeli I, et al. Transcriptional and cellular diversity of the human heart. *Circulation*. 2020;142:466–482. doi: 10.1161/CIRCULATIONAHA.119.045401
6. Seidel T, Navankasattusas S, Ahmad A, Diakos NA, Xu WD, Tristani-Firouzi M, Bonios MJ, Taleb I, Li DY, Selzman CH, et al. Sheet-like remodeling of the transverse tubular system in human heart failure impairs excitation-contraction coupling and functional recovery by mechanical unloading. *Circulation*. 2017;135:1632–1645. doi: 10.1161/CIRCULATIONAHA.116.024470
7. Percie du Sert N, Hurst V, Ahluwalia A, Alam S, Avey MT, Baker M, Browne WJ, Clark A, Cuthill IC, Dirnagl U, et al. The ARRIVE guidelines 2.0: updated guidelines for reporting animal research. *BMJ Open Sci*. 2020;4:e100115. doi: 10.1111/bph.15193
8. Abuduwufuer K, Wang JJ, Li H, Chen C. A modified technique for transverse aortic constriction in mice. *J Vis Exp*. 2022;e64386. doi: 10.3791/64386
9. Bosch L, de Haan JJ, Bastemeijer M, van der Burg J, van der Worp E, Wesseling M, Viola M, Odille C, El Azzouzi H, Pasterkamp G, et al. The transverse aortic constriction heart failure animal model: a systematic review and meta-analysis. *Heart Fail Rev*. 2021;26:1515–1524. doi: 10.1007/s10741-020-09960-w
10. Juan F, Wei D, Xiongzhi Q, Ran D, Chunmei M, Lan H, Chuan Q, Lianfeng Z. The changes of the cardiac structure and function in cTnTR141W transgenic mice. *Int J Cardiol*. 2008;128:83–90. doi: 10.1016/j.ijcard.2008.03.006
11. Ramratnam M, Salama G, Sharma RK, Wang DWR, Smith SH, Banerjee SK, Huang XN, Gifford LM, Pruce ML, Gabris BE, et al. Gene-targeted mice with the human troponin T R141W mutation develop dilated cardiomyopathy with calcium desensitization. *PLoS One*. 2016;11:e0167681. doi: 10.1371/journal.pone.0167681
12. Chang Y, Li X, Cheng Q, Hu Y, Chen X, Hua X, Fan X, Tao M, Song J, Hu S. Single-cell transcriptomic identified HIF1A as a target for attenuating acute rejection after heart transplantation. *Basic Res Cardiol*. 2021;116:64. doi: 10.1007/s00395-021-00904-5
13. Li A, Ponten F, dos Remedios CG. The interactome of LIM domain proteins: the contributions of LIM domain proteins to heart failure and heart development. *Proteomics*. 2012;12:203–225. doi: 10.1002/pmic.201100492
14. Gammons J, Halpage J, Mancarella S. Mapping the proximity interaction network of STIM1 reveals new mechanisms of cytoskeletal regulation. *Cells*. 2021;10:2701. doi: 10.3390/cells10102701
15. Dummler B, Tschopp O, Hynx D, Yang ZZ, Dirnhofer S, Hemmings BA. Life with a single isoform of Akt: mice lacking Akt2 and Akt3 are viable but display impaired glucose homeostasis and growth deficiencies. *Mol Cell Biol*. 2006;26:8042–8051. doi: 10.1128/MCB.00722-06
16. Chen JL, Merl D, Peterson CW, Wu J, Liu PY, Yin H, Muoio DM, Ayer DE, West M, Chi JT. Lactic acidosis triggers starvation response with paradoxical induction of TXNIP through MondoA. *PLoS Genet*. 2010;6:e1001093. doi: 10.1371/journal.pgen.1001093
17. Litvinukova M, Talavera-Lopez C, Maatz H, Reichart D, Worth CL, Lindberg EL, Kanda M, Polanski K, Heinig M, Lee M, et al. Cells of the adult human heart. *Nature*. 2020;588:466–472. doi: 10.1038/s41586-020-2797-4
18. Towler MC, Hardie DG. AMP-activated protein kinase in metabolic control and insulin signaling. *Circ Res*. 2007;100:328–341. doi: 10.1161/01.RES.0000256090.42690.05
19. Bookwalter CS, Trybus KM. Functional consequences of a mutation in an expressed human alpha-cardiac actin at a site implicated in familial hypertrophic cardiomyopathy. *J Biol Chem*. 2006;281:16777–16784. doi: 10.1074/jbc.M512935200
20. Ku HJ, Ahn Y, Lee JH, Park KM, Park JW. IDH2 deficiency promotes mitochondrial dysfunction and cardiac hypertrophy in mice. *Free Radic Biol Med*. 2015;80:84–92. doi: 10.1016/j.freeradbiomed.2014.12.018
21. Hendrickx JO, De Moudt S, Van Dam D, De Deyn PP, Fransen P, De Meyer GRY. Altered stress hormone levels affect in vivo vascular function in the hAPP23(±) overexpressing mouse model of Alzheimer's disease. *Am J Physiol Heart Circ Physiol*. 2021;321:H905–HH19. doi: 10.1152/ajpheart.00254.2021
22. Gupta M, Sueblinvong V, Raman J, Jeevanandam V, Gupta MP. Single-stranded DNA-binding proteins PURalpha and PURbeta bind to a purine-rich negative regulatory element of the alpha-myosin heavy chain gene and control transcriptional and translational regulation of the gene expression. Implications in the repression of alpha-myosin heavy chain during heart failure. *J Biol Chem*. 2003;278:44935–44948. doi: 10.1074/jbc.M307696200
23. Antzelevitch C, Pollevick GD, Cordeiro JM, Casis O, Sanguinetti MC, Aizawa Y, Guerchicoff A, Pfeiffer R, Oliva A, Wollnik B, et al. Loss-of-function mutations in the cardiac calcium channel underlie a new clinical entity characterized by ST-segment elevation, short QT intervals, and sudden cardiac death. *Circulation*. 2007;115:442–449. doi: 10.1161/CIRCULATIONAHA.106.668392
24. Freeman KW, Bowman BR, Zetter BR. Regenerative protein thymosin beta-4 is a novel regulator of purinergic signaling. *FASEB J*. 2011;25:907–915. doi: 10.1096/fj.10-169417

25. Duan R, Liu Y, Tang D, Xiao S, Lin R, Zhao M. Single-cell RNA-Seq reveals CVI-mAb-induced Lyve1^{+} M2-like macrophages reduce atherosclerotic plaque area in Apoe$^{-/-}$ mice. *Int Immunopharmacol*. 2023;116:109794. doi: 10.1016/j.intimp.2023.109794
26. Di YX, Bao YJ, Zhu ZQ, Sun SL, Tian FX, Wang FR, Yu G, Zhang MF, Han J, Zhou LL. Tomentosin suppressed M1 polarization via increasing MERTK activation mediated by regulation of GAS6. *J Ethnopharmacol*. 2023;314:116429. doi: 10.1016/j.jep.2023.116429
27. Hu N, Zou L, Wang C, Song G. RUNX1T1 function in cell fate. *Stem Cell Res Ther*. 2022;13:369. doi: 10.1186/s13287-022-03074-w
28. Yun N, Nah J, Lee MN, Wu D, Pae M. Post-effects of time-restricted feeding against adipose tissue inflammation and insulin resistance in obese mice. *Nutrients*. 2023;15:2617. doi: 10.3390/nu15112617
29. O'Rourke SA, Dunne A, Monaghan MG. The role of macrophages in the infarcted myocardium: orchestrators of ECM remodeling. *Front Cardiovasc Med*. 2019;6:101. doi: 10.3389/fcvm.2019.00101
30. Melnick AM, Westendorf JJ, Polinger A, Carlile GW, Arai S, Ball HJ, Lutterbach B, Hiebert SW, Licht JD. The ETO protein disrupted in t(8;21)-associated acute myeloid leukemia is a corepressor for the promyelocytic leukemia zinc finger protein. *Mol Cell Biol*. 2000;20:2075–2086. doi: 10.1128/MCB.20.6.2075-2086.2000
31. Namekata K, Guo X, Kimura A, Azuchi Y, Kitamura Y, Harada C, Harada T. Roles of the DOCK-D family proteins in a mouse model of neuroinflammation. *J Biol Chem*. 2020;295:6710–6720. doi: 10.1074/jbc.RA119.010438
32. Tripathi V, Popescu NC, Zimonjic DB. DLC1 suppresses NF-kappaB activity in prostate cancer cells due to its stabilizing effect on adherens junctions. *Springerplus*. 2014;3:27. doi: 10.1186/2193-1801-3-27
33. Sangaletti S, Tripodo C, Cappetti B, Casalini P, Chiodoni C, Piconese S, Santangelo A, Parenza M, Arioli I, Miotti S, et al. SPARC oppositely regulates inflammation and fibrosis in bleomycin-induced lung damage. *Am J Pathol*. 2011;179:3000–3010. doi: 10.1016/j.ajpath.2011.08.027
34. Deng SK, Jin Y, Jin Y, Wang JF. SPARC induces M2 polarization of macrophages to promote proliferation, migration, and angiogenesis of cholangiocarcinoma cells. *Neoplasma*. 2022;69:1101–1107. doi: 10.4149/neo_2022_220324N333
35. Hu S, Liu Y, You T, Zhu L. Semaphorin 7A promotes VEGFA/VEGFR2-mediated angiogenesis and intraplaque neovascularization in *ApoE*$^{-/-}$ mice. *Front Physiol*. 2018;9:1718. doi: 10.3389/fphys.2018.01718
36. Stenger S, Hanson DA, Teitelbaum R, Dewan P, Niazi KR, Froelich CJ, Ganz T, Thoma-Uszynski S, Melián A, Bogdan C, et al. An antimicrobial activity of cytolytic T cells mediated by granulysin. *Science*. 1998;282:121–125. doi: 10.1126/science.282.5386.121
37. Febbraio M, Hajjar DP, Silverstein RL. CD36: a class B scavenger receptor involved in angiogenesis, atherosclerosis, inflammation, and lipid metabolism. *J Clin Invest*. 2001;108:785–791. doi: 10.1172/JCI14006
38. Xu Y, Wei K, Kulyk W, Gong SG. FLRT2 promotes cellular proliferation and inhibits cell adhesion during chondrogenesis. *J Cell Biochem*. 2011;112:3440–3448. doi: 10.1002/jcb.23271
39. Marchesi C, Essalmani R, Lemarie CA, Leibovitz E, Ebrahimian T, Paradis P, Seidah NG, Schiffrin EL, Prat A. Inactivation of endothelial proprotein convertase 5/6 decreases collagen deposition in the cardiovascular system: role of fibroblast autophagy. *J Mol Med (Berl)*. 2011;89:1103–1111. doi: 10.1007/s00109-011-0776-9
40. Surapisitchat J, Jeon KI, Yan C, Beavo JA. Differential regulation of endothelial cell permeability by cGMP via phosphodiesterases 2 and 3. *Circ Res*. 2007;101:811–818. doi: 10.1161/CIRCRESAHA.107.154229
41. Bedi KC Jr, Snyder NW, Brandimarto J, Aziz M, Mesaros C, Worth AJ, Wang LL, Javaheri A, Blair IA, Margulies KB, et al. Evidence for intramyocardial disruption of lipid metabolism and increased myocardial ketone utilization in advanced human heart failure. *Circulation*. 2016;133:706–716. doi: 10.1161/CIRCULATIONAHA.115.017545
42. Amorim PA, Nguyen TD, Shingu Y, Schwarzer M, Mohr FW, Schrepper A, Doenst T. Myocardial infarction in rats causes partial impairment in insulin response associated with reduced fatty acid oxidation and mitochondrial gene expression. *J Thorac Cardiovasc Surg*. 2010;140:1160–1167. doi: 10.1016/j.jtcvs.2010.08.003
43. Zalman Y, Klipper E, Farberov S, Mondal M, Wee G, Folger JK, Smith GW, Meidan R. Regulation of angiogenesis-related prostaglandin f2alpha-induced genes in the bovine corpus luteum. *Biol Reprod*. 2012;86:92. doi: 10.1095/biolreprod.111.095067
44. McClelland M, Zhao L, Carskadon S, Arenberg D. Expression of CD74, the receptor for macrophage migration inhibitory factor, in non-small cell lung cancer. *Am J Pathol*. 2009;174:638–646. doi: 10.2353/ajpath.2009.080463
45. Shibuya M, Claesson-Welsh L. Signal transduction by VEGF receptors in regulation of angiogenesis and lymphangiogenesis. *Exp Cell Res*. 2006;312:549–560. doi: 10.1016/j.yexcr.2005.11.012
46. Xi NM, Li JJ. Benchmarking computational doublet-detection methods for single-cell RNA sequencing data. *Cell Syst*. 2021;12:176–194.e6. doi: 10.1016/j.cels.2020.11.008